ALIX-CHMP4 interactions in the human ESCRT pathway

John McCullough, Robert D. Fisher, Frank G. Whitby, Wesley I. Sundquist*, and Christopher P. Hill*

Department of Biochemistry, University of Utah, Salt Lake City, UT 84112-5650.

Edited by Axel T. Brunger, Stanford University, Stanford, CA, and approved March 25, 2008 (received for review February 16, 2008)

The ESCRT pathway facilitates membrane fission events during enveloped virus budding, multivesicular body formation, and cytokinesis. To promote HIV budding and cytokinesis, the ALIX protein must bind and recruit CHMP4 subunits of the ESCRT-III complex, which in turn participate in essential membrane remodeling functions. Here, we report that the Bro1 domain of ALIX binds specifically to C-terminal residues of the human CHMP4 proteins (CHMP4A-C). Crystal structures of the complexes reveal that the CHMP4 C-terminal peptides form amphipathic helices that bind across the conserved concave surface of $ALIX_{Bro1}$. ALIX-dependent HIV-1 budding is blocked by mutations in exposed $ALIX_{Bro1}$ residues that help contribute to the binding sites for three essential hydrophobic residues that are displayed on one side of the CHMP4 recognition helix (M/L/IxxLxxW). The homologous CHMP1–3 classes of ESCRT-III proteins also have C-terminal amphipathic helices, but, in those cases, the three hydrophobic residues are arrayed with L/I/MxxxLxxL spacing. Thus, the distinct patterns of hydrophobic residues provide a ''code'' that allows the different ESCRT-III subunits to bind different ESCRT pathway partners, with CHMP1–3 proteins binding MIT domain-containing proteins, such as VPS4 and Vta1/LIP5, and CHMP4 proteins binding Bro1 domain-containing proteins, such as ALIX.

cytokinesis | ESCRT-III | HIV | mutivesicular body

The ESCRT pathway functions in the budding of HIV-1 and other lentiviruses (1), in the final abscission stage of cytokinesis (2), and in intralumenal vesicle formation at the late endosome or multivesicular body (MVB) (3, 4). Involvement in these seemingly diverse biological processes can be rationalized if the ESCRT machinery encodes membrane remodeling and fission activities that are required to resolve the thin membrane ''necks'' created during the final stages of virus budding, MVB vesicle formation, and cell division. Although mechanistic details are still lacking, there is increasing evidence that the ESCRT-III proteins may mediate such vesicle extrusion and/or membrane fission activities, possibly in conjunction with the AAA ATPase VPS4 (for example, see ref. 5). Humans express 11 related, but distinct ESCRT-III proteins (termed the CHMP proteins) that can be subdivided into seven different families (CHMP1–7) based on their similarities to one another and to the six ESCRT-III-like proteins in yeast. The different ESCRT-III proteins apparently adopt similar folds (6) and can copolymerize together on membranes, yet have evolved to interact differently with other ESCRT pathway components. For example, only the three human CHMP4 proteins (CHMP4A-C) can bind ALIX (yeast Bro1p), another protein in the ESCRT pathway (7–16).

The ESCRT machinery functions at different membranes, and ALIX plays important roles in targeting the pathway to function in retrovirus budding by binding directly to viral Gag proteins (16, 17) and to function in abscission by binding the midbody protein CEP55 (2). In both cases, ALIX must also bind the CHMP4 proteins, because ALIX point mutations that block CHMP4 binding inhibit HIV-1 budding (10, 11) and abscission (18). Thus, ALIX can serve as an adaptor that recruits CHMP4/ESCRT-III complexes to function at distinct biological membranes. Conversely, CHMP4 proteins can apparently recruit ALIX to membranes because the membrane-bound Snf7p (yeast CHMP4) brings Bro1p/ALIX to the endosome to function in MVB vesicle formation (19).

In addition to its involvement in HIV budding and cytokinesis, ALIX has been implicated in a variety of biological processes that may reflect other ESCRT pathway functions or possibly ESCRT-independent ALIX functions. These functions include lysobisphosphatidic acid (LBPA) binding (reviewed in ref. 20), endophilin binding (21), receptor trafficking (22–24), endosome distribution (25), cell motility/adhesion (26, 27), apoptosis (reviewed in ref. 28), actin and microtubule binding (26, 29) and regulation of JNK signaling (30). Thus, ALIX appears to play widespread roles in membrane biology and cell signaling. Similarly, ALIX has been implicated in the release of several other classes of enveloped viruses, including hepatitis B virus (31), human parainfluenza virus (32), and possibly Sendai virus (33) (however, see ref. 34). Thus, ALIX may play widespread roles in the release of highly divergent enveloped viruses.

ALIX has three distinct regions: an N-terminal Bro1 domain (residues 1–358), a central ''V'' domain (362–702), and a C-terminal proline-rich region (703–868). Crystal structures of different ALIX constructs (9, 10, 35) have revealed that the banana-shaped Bro1 domain is organized about a core of tetratricopeptide helical hairpins and that the V domain is composed of two extended helical arms that fold in the shape of the letter V. $YP(X_n)L$ sequence motifs within retroviral Gag proteins bind on the inner face of the second arm of the V domain (10, 17, 35–37). The proline-rich region contains binding epitopes for a number of other cellular factors, including TSG101 (13, 15, 16), endophilins (21), and ALG-2 (38, 39). The Bro1 domain contains binding sites for both HIV-1 NC (40) and the CHMP4 proteins (7–11). Mutations that inhibit CHMP4 binding cluster within an exposed hydrophobic patch on the concave surface of the Bro1 domain, which is thought to be the CHMP4 binding site (9–11). This important interaction has yet to be characterized in molecular detail, however, and, we have therefore mapped the ALIX binding sites on the three human CHMP4 proteins and determined crystal structures of the relevant $ALIX_{Bro1}$-CHMP4 complexes.

Results

CHMP4-ALIX Interactions. Deletion analyses were used in conjunction with biosensor binding experiments to map the ALIX

Author contributions: J.M. and R.D.F. contributed equally to this work; J.M., R.D.F., W.I.S., and C.P.H. designed research; J.M., R.D.F., and F.G.W. performed research; and J.M., W.I.S., and C.P.H. wrote the paper.

The authors declare no conflict of interest.

This article is a PNAS Direct Submission.

Data deposition: The atomic coordinates and structure factors have been deposited in the Protein Data Bank, www.pdb.org [ID codes 3C3O (CHMP4A), 3C3Q (CHMP4B), and 3C3R (CHMP4C)].

*To whom correspondence may be addressed. E-mail: wes@biochem.utah.edu or chris@biochem.utah.edu.

This article contains supporting information online at www.pnas.org/cgi/content/full/0801567105/DCSupplemental.

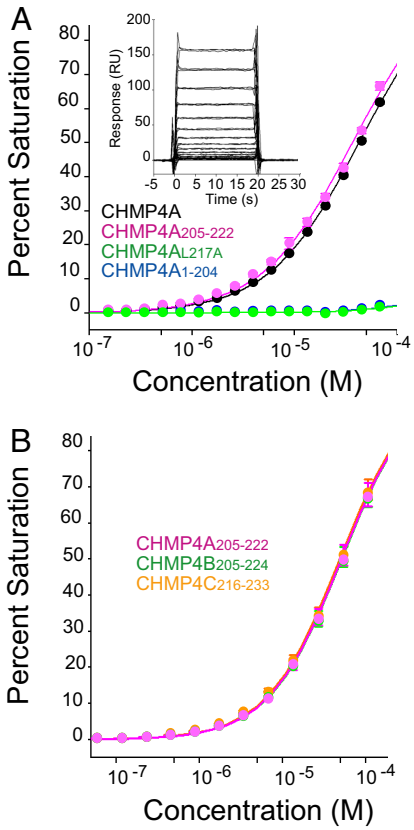

Fig. 1. Mapping the ALIX binding sites of CHMP4 proteins. (*A*) Binding isotherms and sensorgrams (*Inset*) showing $ALIX_{Bro1-V}$ binding to GST-CHMP4A (K_D = 30 ± 11 μM) (*Inset*), GST-$CHMP4A_{205-222}$ (K_D = 44 ± 6 μM), GST-$CHMP4A_{L217A}$ (binding not detectable), and GST-$CHMP4A_{1-204}$ (binding not detectable). The K_D estimates are averages from best fits to single-site binding models (mean ± SD, $n \geq 3$). The shorter $ALIX_{Bro1}$ construct also bound to $CHMP4A_{205-222}$ (K_D = 40 ± 0.6 μM) and to the longer $CHMP4A_{195-222}$ (K_D = 40.5 ± 0.4 μM) and $CHMP4A_{174-222}$ (K_D = 36.5 ± 0.4 μM) C-terminal constructs with comparable affinities (dissociation constant and error were estimated from a statistical fit of a single binding isotherm derived from duplicate measurements at 10 different $ALIX_{Bro1-V}$ concentrations; data not shown). Error bars are indicated on all biosensor figures, but are often too small to be readily visible. (*B*) $ALIX_{Bro1}$ binds the C termini of CHMP4A, CHMPB, and CHMP4C. Binding isotherms showing $ALIX_{Bro1-V}$ binding to immobilized C-terminal peptides from CHMP4A-C. Estimated dissociation constants were: GST-$CHMP4A_{205-222}$, 44 ± 6 μM (mean ± SD, n = 6); GST-$CHMP4B_{205-224}$, 48 ± 6 μM (mean ± range, n = 2); GST-$CHMP4C_{216-233}$, 41 ± 10 μM (mean ± range, n = 2). Binding to a control GST surface was negligible (data not shown).

binding site on CHMP4A. As summarized in Fig. 1*A*, an ALIX construct spanning the Bro1 and V domains ($ALIX_{Bro1-V}$) bound both full-length CHMP4A and a minimal C-terminal $CHMP4A_{205-222}$ construct with similar affinities (30 ± 11 μM and 44 ± 6 μM), but did not bind detectably to a CHMP4A construct that lacked the final 18 residues ($CHMP_{1-204}$) or to a full-length CHMP4A protein that harbored a single point mutation within this region ($CHMP4A_{L217A}$) (15). Thus, the $ALIX_{Bro1-V}$ binding site maps to the final 18 residues of CHMP4A.

The three human CHMP4 family members have similar but distinct C-terminal sequences, so we tested whether peptides corresponding to the termini of CHMP4B and CHMP4C also bound $ALIX_{Bro1-V}$. As shown in Fig. 1*B*, terminal fragments from all three CHMP4 proteins bound $ALIX_{Bro1-V}$ with similar affinities (44, 48, and 41 μM, respectively), demonstrating that all three CHMP4 proteins encode C-terminal ALIX binding sites. Similar binding data were also obtained for the shorter

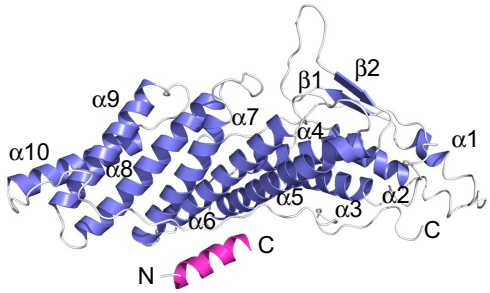

Fig. 2. Ribbon diagram showing the $ALIX_{Bro1}$ domain (blue) in complex with the C-terminal helix from CHMP4A (purple).

$ALIX_{Bro1}$ construct (see Fig. 1 legend), and the Bro1 domain of ALIX, therefore, binds the C termini of all three human CHMP4 proteins.

Crystal Structures of $ALIX_{Bro1}$-CHMP4 Complexes. Crystal structures of $ALIX_{Bro1}$ in complex with peptides corresponding to the C-terminal binding sites from each of the three human CHMP4 proteins were determined in order to visualize the molecular basis for ALIX-CHMP4 interactions [Figs. 2 and 3 and supporting information (SI) Figs. S1–S3]. All three complexes crystallized isomorphously in space group C2 with a single $ALIX_{Bro1}$-CHMP4 complex in the asymmetric unit. The CHMP4A-C complexes were refined to resolutions of 2.15, 2.10, and 2.02 Å, respectively, with good geometries and R_{free} values <30% (Table S1).

As shown in Fig. 2, $CHMP4A_{205-222}$ forms an amphipathic helix that binds across the concave surface of $ALIX_{Bro1}$, con-

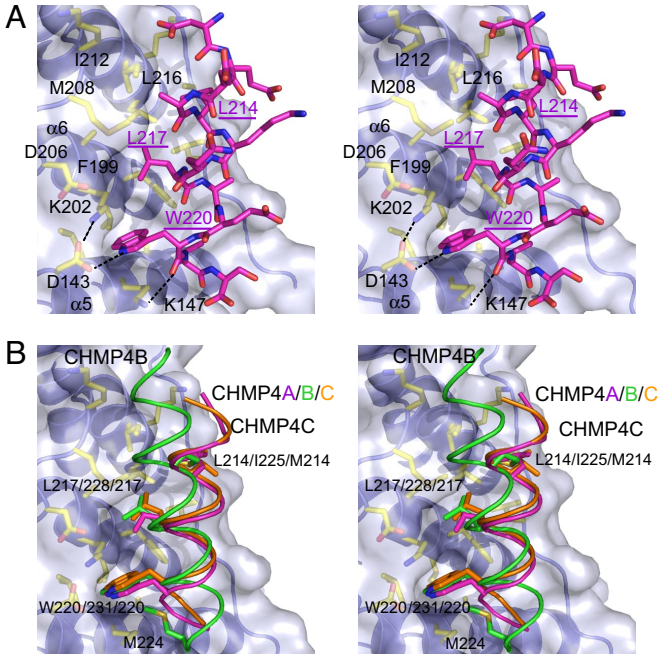

Fig. 3. $ALIX_{Bro1}$-CHMP4 interfaces. (*A*) Stereoview of the $ALIX_{Bro1}$-CHMP4A interface. The CHMP4A helix is oriented N to C from top to bottom, ALIX residues within the binding interface are shown explicitly, dashed lines indicate hydrogen bonds or salt bridges, and key hydrophobic CHMP4 residues are underlined. (*B*) Stereo-view showing an overlay of the bound CHMP4A-C helices. The orientation is the same as in *A*, and the three key hydrophobic CHMP4 binding residues are shown in sticks. Note that the CHMP4A (purple) and CHMP4C (orange) helices overlay well, whereas the CHMP4B helix (green) is rotated by ≈20°.

tacting helices 5–7 and the extended C-terminal strand that traverses the domain. $ALIX_{Bro1}$ does not change conformation notably upon CHMP4 binding, although several sidechains in the binding site shift slightly, with the largest adjustment (≈1.5Å) being made by the ALIX Phe-199 ring. The $CHMP4A_{205-222}$ and $CHMP4C_{216-233}$ peptides have similar lengths and sequences and bind $ALIX_{Bro1}$ in very similar fashions, whereas the longer $CHMP4B_{205-224}$ peptide binds at the same site, but in a slightly different fashion (see below).

In all three complexes, important interactions are made by hydrophobic residues located on three successive turns of the CHMP4 recognition helix (CHMP4A residues Leu-214, Leu-217, and Trp-220). The most distinctive contact is made by the indole ring of Trp-220, which binds in a hydrophobic pocket located between helices 5 and 6 (Fig. 3*A*). The indole nitrogen also forms a hydrogen bond with the conserved ALIX Asp-143 carboxylate, which in turn is buttressed by a salt bridge with the ALIX Lys-202 side chain. Leu-217 binds in an adjacent hydrophobic pocket located between ALIX helices 6 and 7, whereas Leu-214 binds on a more open hydrophobic surface of ALIX helix 6. No other CHMP4A side chains make substantial contacts, and the structures therefore indicate that the three hydrophobic residues of the CHMP4A recognition helices are the primary determinants of ALIX binding and specificity. The terminal carboxylates of CHMP4A and CHMP4C probably also contribute to ALIX recognition, because they make water-mediated interactions with the ALIX Lys-151 side chain.

The $ALIX_{Bro1}$-$CHMP4B_{205-224}$ Complex. The longer $CHMP4B_{205-224}$ peptide binds $ALIX_{Bro1}$ at the same site and forms an amphipathic helix that places the same three hydrophobic side chains in analogous binding sites. In this case, however, the helix is rotated by ≈20° relative to the CHMP4A/C helices, which displaces the N and C termini of the CHMP4B helix by ≈5Å and 3Å, respectively. (Fig. 3*B* and Figs. S2*B* and S3). The C-terminal displacement allows the final two CHMP4B residues (not present in the shorter CHMP4A/C helices) to make unique interactions that appear to dictate the helix orientation. Specifically, the CHMP4B Ser-223 hydroxyl caps the helix and hydrogen bonds with the ALIX Lys-147 side chain (whereas ALIX Lys-147 hydrogen bonds with the Trp-220 main-chain carbonyl in the CHMP4A and 4C complexes). The terminal CHMP4B Met-224 residue, in turn, contacts a hydrophobic patch between ALIX helices 5 and 6 (Fig. 3*B* and Fig. S3*B*). Thus, the C-terminal helices of all three human CHMP4 proteins bind the same site on ALIX, although the detailed interactions can differ depending on the length of the recognition helix.

Mutational Analyses of the $ALIX_{Bro1}$-CHMP4A Interaction. Biosensor binding assays were also performed to test the importance of the three conserved hydrophobic residues of the CHMP4 recognition helix. As shown in Fig. 4*A*, single alanine substitutions of CHMP4A residues Leu-214, Leu-217, and Trp-220 abolished $ALIX_{Bro1-V}$ binding, confirming the energetic importance of all three residues. A cluster of acidic residues is also conserved at the N-terminal end of the CHMP4 recognition helix (Fig. 4*B*). These residues do not contact ALIX directly in the crystal structures, but do approach basic surface residues Lys-209 and Lys-215, and could therefore also contribute to binding. Mutation of the glutamate residue present in all three human CHMP4 proteins (CHMP4A Glu-209) reduced $ALIX_{Bro1-V}$ binding affinity by twofold, indicating that hydrophilic flanking residues can also contribute to $ALIX_{Bro1}$ binding, albeit modestly.

Discussion

Our biochemical and structural analyses show that ALIX binds amphipathic C-terminal helices on all three human CHMP4 proteins. Three hydrophobic residues on the CHMP4 recognition

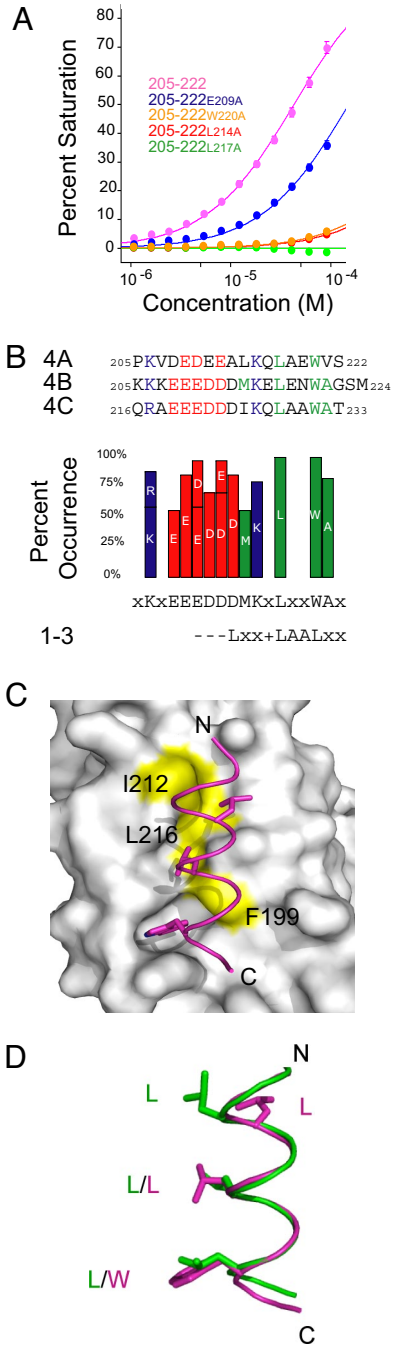

Fig. 4. Molecular recognition in ALIX-CHMP4 complexes. (*A*) Isotherms showing $ALIX_{Bro1-V}$ binding to immobilized WT $CHMP4A_{205-222}$ and to $CHMP4A_{205-222}$ constructs with the following mutations: W220A, L217A, L214A, and E209A. For the E209A mutant, K_D = 95 ± 2 μM (dissociation constant and error were estimated from a statistical fit of a single binding isotherm derived from duplicate measurements at 10 different $ALIX_{Bro1-V}$ concentrations.). (*B*) Sequences of the C termini of human CHMP4 proteins are shown (*Upper*), together with a bar graph showing sites of >50% identity across metazoan CHMP4 proteins, the resulting CHMP4 consensus sequence (see also Table S2) and the distinct consensus sequence of the C-terminal amphipathic helices of CHMP1–3 proteins (*Lower*) (47). (*C*) Model of the $ALIX_{Bro1}$-CHMP4A interaction, with mutation sites that block ALIX binding and ALIX-dependent HIV-1 budding highlighted in yellow on the ALIX surface. (*D*) Overlay of the C-terminal recognition helices from CHMP4A (magenta) and CHMP1A (green, PDB 2jq9), extracted from the bound $ALIX_{Bro1}$-$CHMP4A_{205-222}$ and VPS4A MIT-$CHMP1A_{180-196}$ complexes. The three key hydrophobic residues from each recognition helix are shown explicitly, and the figure emphasizes that the first hydrophobic residue is positioned differently in the two helices.

helices contact ALIX extensively, and their energetic importance was confirmed by mutagenesis. The C-terminal Leu and Trp residues are invariant in metazoan CHMP4 proteins, whereas the first hydrophobic position of the helix can vary between Met, Leu, Ile, and Phe (Fig. 4*B* and Table S2). This pattern of conservation is nicely explained by the $ALIX_{Bro1}$-CHMP4 structures, which show that the terminal Leu and Trp residues of the CHMP4 recognition helix bind in well defined pockets, whereas the first hydrophobic residue in the helix binds against a flat hydrophobic surface that can presumably tolerate greater side chain variability. Several sets of flanking hydrophilic residues are also conserved in the recognition helix, including an upstream acidic cluster (residues 208–212 in CHMP4A) and two basic residues (CHMP4A Lys-206 and 215). These side chains are solvent exposed and do not contact ALIX extensively, but a mutation within the CHMP4A acidic cluster did reduce $ALIX_{Bro1}$ binding slightly, indicating that the cluster may interact favorably with the basic $ALIX_{Bro1}$ surface. It is alternatively possible, however, that flanking hydrophilic residues are conserved primarily because they make important contacts when CHMP4 proteins adopt alternative conformations or bind other partners.

CHMP4 binding appears to be a conserved function of Bro1 domains, because three other Bro1 domain-containing proteins, Rim20p, HD-PTP, and Brox, also bind CHMP4 proteins (41, 42). Alignment of the Bro1 domains from metazoan ALIX proteins, human Brox and HD-PTP, and yeast Rim20p and Bro1p reveal strong, although not absolute conservation of CHMP4 contact residues, suggesting that most Bro1 domains will bind CHMP4 proteins in a similar fashion (Fig. S4). For example, the $ALIX_{Bro1}$ Asp-143 and Lys-202 residues, which form a salt bridge that buttresses the $ALIX_{Bro1}$ Asp-143-CHMP4A Trp-220 hydrogen bond, are absolutely conserved as an acidic/basic residue pair in all of the aligned Bro1 domains.

ALIX can be recruited to facilitate enveloped virus budding and release, and this function has been studied most extensively for HIV-1 (10, 11). These studies have identified three different ALIX point mutations (F199D, I212D, and L216D) that block both CHMP4 binding and ALIX-mediated release of HIV-1 constructs that cannot recruit TSG101/ESCRT-I. All three of these residues map to the CHMP4 binding interface, and the crystal structures are consistent with the observed loss of CHMP4 binding for Asp mutations at these positions (Fig. 4*C*). The ALIX I212D mutation has also been shown to block the ALIX-dependent abscission step of cytokinesis (18). Thus, the crystallographic ALIX-CHMP4 interface visualized here is essential for ALIX-dependent steps in HIV-1 budding and cytokinesis. This interaction recruits CHMP4 proteins, which in turn presumably recruit additional ESCRT-III subunits and VPS4 complexes to function in membrane remodeling and fission.

The recruiting order appears to be reversed in the case of MVB vesicle formation, where copolymerization of the different ESCRT-III subunits on endosomal membranes creates a surface that recruits other ESCRT pathway proteins, including ALIX, VPS4, Doa4p, IST1, and Vta1p/LIP5. Like the CHMP4 subunits, the CHMP1–3 subunits of ESCRT-III also have C-terminal amphipathic helices [MIT interacting motifs (MIM)], but in these cases the helices bind the MIT domains of VPS4, Vta1p/LIP5, and AMSH and thereby recruit ATPase and deubiquitylating activities to the membrane (43–48). Hence, the terminal helices of different ESCRT-III subunits must display distinct binding surfaces to ensure specificity in protein recruitment. This is borne out by the observation that the C-terminal CHMP4A helix binds $ALIX_{Bro1}$ but not the VPS4A MIT domain, whereas the C-terminal CHMP1B helix binds the VPS4A MIT domain but not $ALIX_{Bro1}$ (Fig. S5). As shown in Fig. 4*D*, the MIM helices of the CHMP1–3 proteins display three key leucine/hydrophobic residues that make important MIT domain contacts (47, 48). In these cases, the three hydrophobic residues are spaced by three and two intervening residues, whereas the three hydrophobic residues of the CHMP4 recognition helix are each separated by two intervening residues. As a result, the initial hydrophobic residues of the CHMP1–3 and CHMP4 recognition helices occupy different relative positions. Furthermore, the terminal hydrophobic CHMP4 residue is a Trp, whereas the terminal CHMP1–3 hydrophobic residue is a Leu. Thus, the different identities and positions of the hydrophobic residues in their terminal recognition helices help ensure that each ESCRT-III subunit recruits its proper binding partner(s).

Methods

Expression Constructs and Plasmids. Expression constructs for GST-CHMP4A (WISP06–197) and GST-CHMP4A L217A (WISP06–61) are described in ref. 15. Quikchange mutagenesis (Stratagene) was used to create expression constructs for GST-$CHMP4A_{1-204}$ (WISP06–198), GST-$CHMP4A_{205-222}$ (WISP06–60), GST-$CHMP4B_{205-224}$ (WISP06–201), GST-$CHMP4C_{216-233}$ (WISP06–202), GST-$CHMP4A_{205-222W220A}$ (WISP06–203), GST-$CHMP4A_{205-222L217A}$ (WISP06–204), GST-$CHMP4A_{205-222L214A}$ (WISP06–205), and GST-$CHMP4A_{205-222E209A}$ (WISP06–206), using expression constructs for GST-CHMP4A, GST-CHMP4B (WISP06–199), and GST-CHMP4C (WISP06–200) as templates.

ALIX and CHMP4 Protein Expression and Purification. CHMP4 peptides used for crystallization studies were synthesized with an N-terminal acetyl capping group: $_{205}$PKVDEDEEALKQLAEWVS$_{222}$ (CHMP4A), $_{205}$KKKEEEDDDMKELENWAGSM$_{224}$ (CHMP4B), and $_{216}$QRAEEEDDDIKQLAAWAT$_{233}$ (CHMP4C). $ALIX_{Bro1}$ (residues 1–359) and $ALIX_{Bro1\text{-}V}$ (residues 1–702) proteins used in biosensor and crystallization studies were expressed and purified as described in ref. 10. GST-CHMP4 proteins used in biosensor experiments were expressed in BL21(DE3) Codon$^+$ (RIPL) *Escherichia coli* cells grown in autoinduction media, ZYP-50502 (49). Cells were grown at 37°C for 4 h, then transferred to 23°C or 17°C for growth to saturation. Subsequent purification steps were performed at 4°. Cells from 100 ml of cultures were harvested, resuspended in 4 ml of 20 mM sodium phosphate (pH 7.2), 150 mM NaCl, 5 mM β-mercaptoethanol, and protease inhibitors (Roche Diagnostics) and lysed by the addition of 1 mg/ml lysozyme followed by sonication. The lysate was clarified by centrifugation, and GST-CHMP4 proteins were affinity purified by incubation with 500 μl of glutathione beads in biosensor running buffer [20 mM sodium phosphate (pH 7.2), 150 mM NaCl, 0.01% P20, 0.2 mg/ml BSA, 5 mM β-mercaptoethanol] for 30 min, washed extensively, and eluted with 20 mM reduced glutathione in running buffer.

Biosensor Binding Studies. Binding experiments used Biacore 2000 and T100 optical biosensor instruments. Research-grade CM5 sensor chips were derivatized with anti-GST antibody, using amine coupling, and were used to capture affinity purified GST-CHMP4 proteins or GST alone (reference) at surface densities of 300-3030 response units (RU). Similar binding data were obtained for both $ALIX_{Bro1}$ and $ALIX_{Bro1\text{-}V}$ constructs, but the $ALIX_{Bro1\text{-}V}$ construct was more soluble and therefore allowed more complete sampling of the binding isotherms. Pure $ALIX_{Bro1\text{-}V}$ (diluted in running buffer to the designated concentrations) was injected in duplicate (50 μl/min, 20°C) and binding data were collected at 2 Hz during the 30-s association and dissociation phases. All interactions reached equilibrium rapidly and dissociated within seconds during the dissociation phase, and all were studied at more than one surface density to rule out crowding and mass transport effects. Binding responses at 10–20 sec were fit to simple 1:1 binding isotherms to obtain equilibrium constants.

Crystallization. $ALIX_{Bro1}$-CHMP4 crystals were grown by sitting drop vapor diffusion at 4°C at protein:peptide molar ratios of 1:1.2 at final $ALIX_{Bro1}$ concentrations of 25 mg/ml (CHMP4A) or 23 mg/ml (CHMP4B/C). Crystals grew from drops containing 0.5 μl of protein solution mixed with 0.5 μl of reservoir solution: 15% PEG 8000, 100 mM Na MES (pH 6.5), and 200 mM Na Acetate (CHMP4A) from drops containing 1.2 μl of protein solution mixed with 0.7 μl of reservoir solution [15% PEG 8000, 100 mM Na MES (pH 6.5), 200 mM Na Acetate (CHMP4B)] or from drops containing 1.2 μl of protein solution mixed with 0.7 μl of reservoir solution [10% PEG 2000, 100 mM Na MES (pH 6.5) (CHMP4C)].

Data Collection and Structure Refinement. Crystals were cryoprotected in reservoir solutions made up with 20% glycerol, suspended in nylon loops, and flash frozen in liquid nitrogen. Data were collected on a copper rotating anode generator with confocal optics (Rigaku; MicroMax 007HF) and a Rigaku R-Axis IV image plate (CHMP4B and CHMP4C) and at beam lines 11-1(MAR325, 0.97607 Å wavelength) and 7-1 (Quantum 315, 0.98397 Å wavelength) of the Stanford Synchrotron Radiation Laboratory (CHMP4A). Crystals were maintained at 100 K during data collection. Data were integrated and scaled with

Denzo and Scalepack, using the HKL2000 suite (50). $ALIX_{Bro1}$-CHMP4 crystals were isomorphous with crystals of unliganded $ALIX_{Bro1}$ (PDB entry 2OEW) (10). The unliganded $ALIX_{Bro1}$ structure was used as a starting model for all three refinements, which were performed with REFMAC, using the maximum likelihood target function and incorporating TLS analysis (51, 52) as implemented in the CCP4 package (53). Models were built in O (54) and COOT (55), geometry was analyzed with PROCHECK (56), and figures were generated in PyMOL (57). The following residues were modeled in the different CHMP4 complexes: CHMP4A, 210–222; CHMP4B, 207–224; and CHMP4C, 221–233. Crystallographic statistics are presented in Table S1.

ACKNOWLEDGMENTS. Biosensor analyses were performed at the University of Utah core facility, and x-ray data were collected at the Stanford Synchrotron Radiation Laboratory (SSRL). The SSRL is a national user facility operated by Stanford University on behalf of the U.S. Department of Energy, Office of Basic Energy Sciences. The SSRL Structural Molecular Biology Program is supported by the Department of Energy Office of Biological and Environmental Research, the National Institutes of Health National Center for Research Resources, Biomedical Technology Program, and National Institute of General Medical Sciences. This work was supported by National Institutes of Health Grants GM082534 (to W.I.S. and C.P.H.) and AI051174 (to W.I.S.).

1. Bieniasz PD (2006) Late budding domains and host proteins in enveloped virus release. *Virology* 344:55–63.
2. Carlton JG, Martin-Serrano J (2007) Parallels between cytokinesis and retroviral budding: A role for the ESCRT machinery. *Science* 316:1908–1912.
3. Hurley JH, Emr SD (2006) The ESCRT complexes: Structure and mechanism of a membrane-trafficking network. *Annu Rev Biophys Biomol Struct* 35:277–298.
4. Williams RL, Urbe S (2007) The emerging shape of the ESCRT machinery. *Nat Rev Mol Cell Biol* 8:355–368.
5. Hanson PI, Roth R, Lin Y, Heuser JE (2008) Plasma membrane deformation by circular arrays of ESCRT-III protein filaments. *J Cell Biol* 180:389–402.
6. Muziol T, *et al.* (2006) Structural basis for budding by the ESCRT-III factor CHMP3. *Dev Cell* 10:821–830.
7. Katoh K, *et al.* (2003) The ALG-2-interacting protein Alix associates with CHMP4b, a human homologue of yeast Snf7 that is involved in multivesicular body sorting. *J Biol Chem* 278:39104–39113.
8. Katoh K, Shibata H, Hatta K, Maki M (2004) CHMP4b is a major binding partner of the ALG-2-interacting protein Alix among the three CHMP4 isoforms. *Arch Biochem Biophys* 421:159–165.
9. Kim J, *et al.* (2005) Structural basis for endosomal targeting by the Bro1 domain. *Dev Cell* 8:937–947.
10. Fisher RD, *et al.* (2007) Structural and biochemical studies of ALIX/AIP1 and its role in retrovirus budding. *Cell* 128:841–852.
11. Usami Y, Popov S, Gottlinger HG (2007) Potent rescue of human immunodeficiency virus type 1 late domain mutants by ALIX/AIP1 depends on its CHMP4 binding site. *J Virol* 81:6614–6622.
12. Bowers K, *et al.* (2004) Protein–protein interactions of ESCRT complexes in the yeast *Saccharomyces cerevisiae*. *Traffic* 5:194–210.
13. Martin-Serrano J, Yaravoy A, Perez-Caballero D, Bieniasz PD (2003) Divergent retroviral late-budding domains recruit vacuolar protein sorting factors by using alternative adaptor proteins. *Proc Natl Acad USA* 100:12414–12419.
14. Peck JW, Bowden ET, Burbelo PD (2004) Structure and function of human Vps20 and Snf7 proteins. *Biochem J* 377:693–700.
15. von Schwedler UK, *et al.* (2003) The protein network of HIV budding. *Cell* 114:701–713.
16. Strack B, Calistri A, Craig S, Popova E, Gottlinger HG (2003) AIP1/ALIX is a binding partner for HIV-1 p6 and EIAV p9 functioning in virus budding. *Cell* 114:689–699.
17. Zhai Q, *et al.* (2008) Structural and functional studies of ALIX interactions with YPX(n)L late domains of HIV-1 and EIAV. *Nat Struct Mol Biol* 15:43–49.
18. Morita E, *et al.* (2007) Human ESCRT and ALIX proteins interact with proteins of the midbody and function in cytokinesis. *EMBO J* 26:4215–4227.
19. Odorizzi G, Katzmann DJ, Babst M, Audhya A, Emr SD (2003) Bro1 is an endosome-associated protein that functions in the MVB pathway in *Saccharomyces cerevisiae*. *J Cell Sci* 116:1893–1903.
20. van der Goot FG, Gruenberg J (2006) Intra-endosomal membrane traffic. *Trends Cell Biol* 16:514–521.
21. Chatellard-Causse C, *et al.* (2002) Alix (ALG-2-interacting protein X), a protein involved in apoptosis, binds to endophilins and induces cytoplasmic vacuolization. *J Biol Chem* 277:29108–29115.
22. Geminard C, De Gassart A, Blanc L, Vidal M (2004) Degradation of AP2 during reticulocyte maturation enhances binding of hsc70 and Alix to a common site on TFR for sorting into exosomes. *Traffic* 5:181–193.
23. Schmidt MH, *et al.* (2004) Alix/AIP1 antagonizes epidermal growth factor receptor down-regulation by the Cbl-SETA/CIN85 complex. *Mol Cell Biol* 24:8981–8993.
24. Shi A, *et al.* (2007) A novel requirement for *C. elegans* Alix/ALX-1 in RME-1-mediated membrane transport. *Curr Biol* 17:1913–1924.
25. Cabezas A, Bache KG, Brech A, Stenmark H (2005) Alix regulates cortical actin and the spatial distribution of endosomes. *J Cell Sci* 118:2625–2635.
26. Schmidt MH, Chen B, Randazzo LM, Bogler O (2003) SETA/CIN85/Ruk and its binding partner AIP1 associate with diverse cytoskeletal elements, including FAKs, and modulate cell adhesion. *J Cell Sci* 116:2845–2855.
27. Ichioka F, *et al.* (2005) Identification of Rab GTPase-activating protein-like protein (RabGAPLP) as a novel Alix/AIP1-interacting protein. *Biosci Biotechnol Biochem* 69:861–865.
28. Sadoul R (2006) Do Alix and ALG-2 really control endosomes for better or for worse? *Biol Cell Eur Cell Biol Org* 98:69–77.
29. Pan S, *et al.* (2006) Involvement of the conserved adaptor protein Alix in actin cytoskeleton assembly. *J Biol Chem* 281:34640–34650.
30. Tsuda M, Seong KH, Aigaki T (2006) POSH, a scaffold protein for JNK signaling, binds to ALG-2 and ALIX in *Drosophila*. *FEBS Lett* 580:3296–3300.
31. Watanabe T, *et al.* (2007) Involvement of host cellular multivesicular body functions in hepatitis B virus budding. *Proc Natl Acad USA* 104:10205–10210.
32. Nishio M, Tsurudome M, Ishihara H, Ito M, Ito Y (2007) The conserved carboxyl terminus of human parainfluenza virus type 2 V protein plays an important role in virus growth. *Virology* 362:85–98.
33. Irie T, Shimazu Y, Yoshida T, Sakaguchi T (2007) The YLDL sequence within Sendai virus M protein is critical for budding of virus-like particles and interacts with Alix/AIP1 independently of C protein. *J Virol* 81:2263–2273.
34. Gosselin-Grenet AS, Marq JB, Abrami L, Garcin D, Roux L (2007) Sendai virus budding in the course of an infection does not require Alix and VPS4A host factors. *Virology* 365:101–112.
35. Lee S, Joshi A, Nagashima K, Freed EO, Hurley JH (2007) Structural basis for viral late-domain binding to Alix. *Nat Struct Mol Biol* 14:194–199.
36. Munshi UM, Kim J, Nagashima K, Hurley JH, Freed EO (2007) An Alix fragment potently inhibits HIV-1 budding: Characterization of binding to retroviral YPXL late domains. *J Biol Chem* 282:3847–3855.
37. Vincent O, Rainbow L, Tilburn J, Arst HN Jr, Peñalva MA (2003) YPXL/I is a protein interaction motif recognized by Aspergillus PalA and its human homologue, AIP1/Alix. *Mol Cell Biol* 23:1647–1655.
38. Trioulier Y, *et al.* (2004) Alix, a protein regulating endosomal trafficking, is involved in neuronal death. *J Biol Chem* 279:2046–2052.
39. Shibata H, *et al.* (2004) The penta-EF-hand protein ALG-2 interacts with a region containing PxY repeats in Alix/AIP1, which is required for the subcellular punctate distribution of the amino-terminal truncation form of Alix/AIP1. *J Biochem (Tokyo)* 135:117–128.
40. Popov S, Popova E, Inoue M, Gottlinger HG (2008) Human immunodeficiency virus type 1 Gag engages the Bro1 domain of ALIX/AIP1 through the nucleocapsid. *J Virol* 82:1389–1398.
41. Xu W, Smith FJ, Jr, Subaran R, Mitchell AP (2004) Multivesicular body-ESCRT components function in pH response regulation in *Saccharomyces cerevisiae* and *Candida albicans*. *Mol Biol Cell* 15:5528–5537.
42. Ichioka F, Kobayashi R, Katoh K, Shibata H, Maki M (2008) Brox, a novel farnesylated Bro1 domain-containing protein that associates with charged multivesicular body protein 4 (CHMP4). *Febs J* 275:682–692.
43. Tsang HT, *et al.* (2006) A systematic analysis of human CHMP protein interactions: Additional MIT domain-containing proteins bind to multiple components of the human ESCRT III complex. *Genomics* 88:333–346.
44. Zamborlini A, *et al.* (2006) Release of autoinhibition converts ESCRT-III components into potent inhibitors of HIV-1 budding. *Proc Natl Acad USA* 103:19140–19145.
45. Row PE, *et al.* (2007) The MIT domain of UBPY constitutes a CHMP binding and endosomal localization signal required for efficient epidermal growth factor receptor degradation. *J Biol Chem* 282:30929–30937.
46. Obita T, *et al.* (2007) Structural basis for selective recognition of ESCRT-III by the AAA ATPase Vps4. *Nature* 449:735–739.
47. Stuchell-Brereton MD, *et al.* (2007) ESCRT-III recognition by VPS4 ATPases. *Nature* 449:740–744.
48. Azmi IF, *et al.* (2008) ESCRT-III family members stimulate Vps4 ATPase activity directly or via Vta1. *Dev Cell* 14:50–61.
49. Studier FW (2005) Protein production by auto-induction in high density shaking cultures. *Protein Expr Purif* 41:207–234.
50. Otwinowski Z, Minor W (1997) Processing of X-ray diffraction data collected in oscillation mode. *Methods Enzymol* 276:307–326.
51. Howlin B, Butler SA, Moss DS, Harris GW, Driessen HPC (1993) TLSANL: TLS parameter analysis program for segmented anisotropic refinement of macromolecular structures. *J Appl Crystallogr* 26:622–624.
52. Murshudov GN, Vagin AA, Lebedev A, Wilson KS, Dodson EJ (1999) Efficient anisotropic refinement of macromolecular structures using FFT. *Acta Crystallogr D Biol Crystallogr* 55:247–255.
53. Group CCP (1994) The CCP4 Suite: Programs for protein crystallography. *Acta Crystallogr D* 50:760–763.
54. Jones TA, Zou JY, Cowan SW, Kjeldgaard M (1991) Improved methods for binding protein models in electron density maps and the location of errors in these models. *Acta Crystallogr A* 47 (Pt 2):110–119.
55. Emsley P, Cowtan K (2004) Coot: Model-building tools for molecular graphics. *Acta Crystallogr D* 60:2126–2132.
56. Laskowski RA, Moss DS, Thornton JM (1993) Main-chain bond lengths and bond angles in protein structures. *J Biol* 231:1049–1067.
57. DeLano WL (2002) The PyMOL User's Manual (DeLano Scientific, San Carlos, CA).

Supporting Information

McCullough *et al.* 10.1073/pnas.0801567105

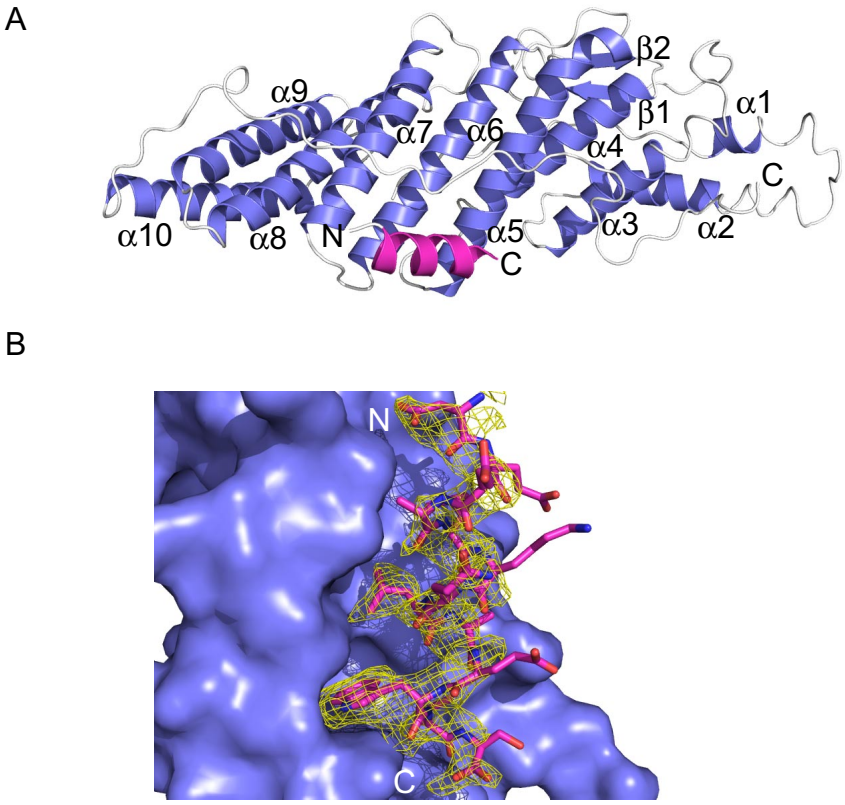

Fig. S1. $ALIX_{Bro1}$ in complex with the C-terminal CHMP4A helix. (*A*) Ribbon diagram showing the complex between $ALIX_{Bro1}$ and the C-terminal helix from CHMP4A (purple). This figure is oriented so that the CHMP4A helix in Fig. 1 *Lower* is rotated ≈90° toward the viewer. (*B*) CHMP4A is represented in sticks against a solid ALIX surface, with the Fo-Fc peptide omit map contoured at 2 × rmsd and displayed over the peptide. To generate the peptide omit map, the peptide was deleted from the model, random shifts (0.3 Å in *x*, *y*, *x*) were applied throughout and the model rerefined without the peptide in REFMAC. The orientation is the same as in Fig. 3.

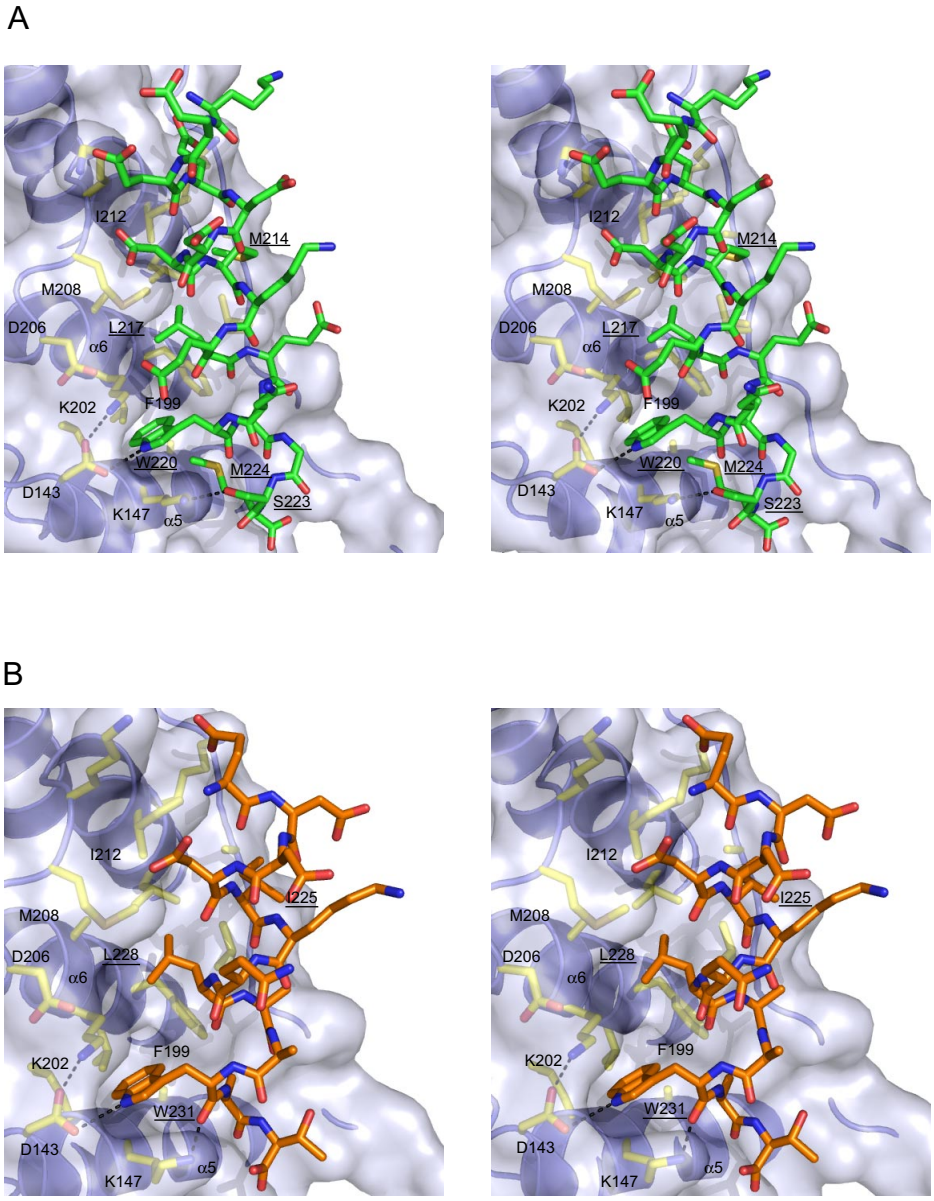

Fig. S2. Stereoviews of $ALIX_{Bro1}$-CHMP4B and $ALIX_{Bro1}$-CHMP4C interfaces. (*A*) $ALIX_{Bro1}$-CHMP4B. (*B*) $ALIX_{Bro1}$-CHMP4C. Views and designations are the same as in Fig. 3*A*, except that CHMP4B is shown in green and CHMP4C is shown in orange.

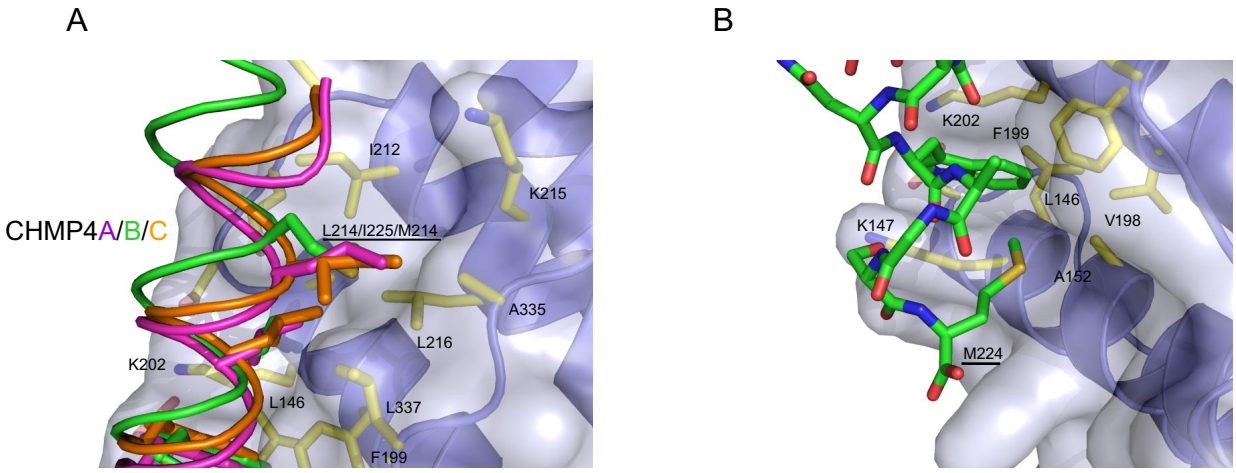

Fig. S3. Comparative analyses of the $ALIX_{Bro1}$-CHMP4B interface. (*A*) Overlay of $ALIX_{Bro1}$-bound CHMP4A-C helices illustrating how hydrophobic residues at the N-terminal ends of the helices can make nearly equivalent contacts despite displacement of the CHMP4B helix (green). (*B*) Expanded view of the CHMP4B C terminus, highlighting the unique $ALIX_{Bro1}$ contacts made by the C-terminal Met-224 residue.

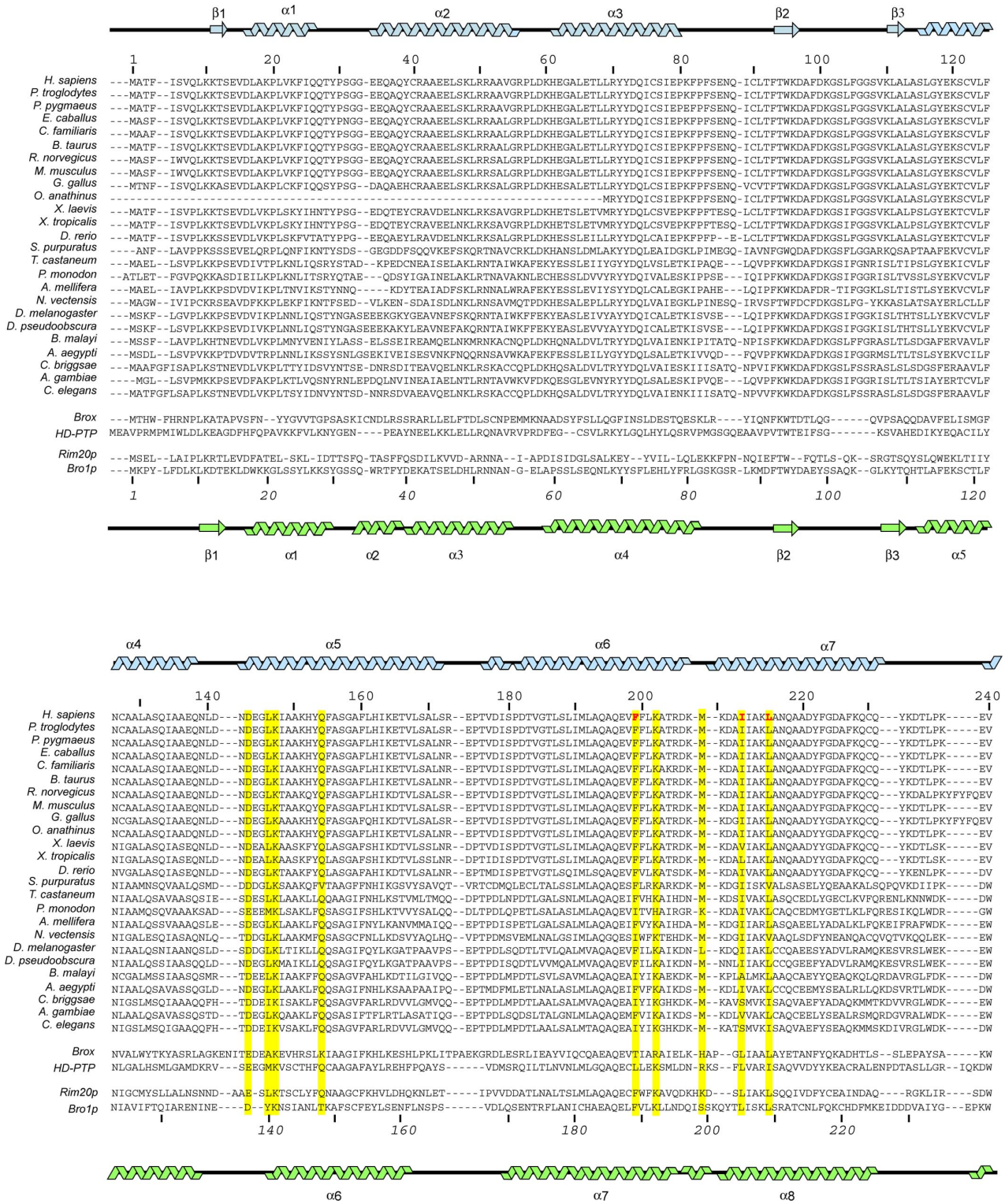

Fig. S4. (Continued on next page.)

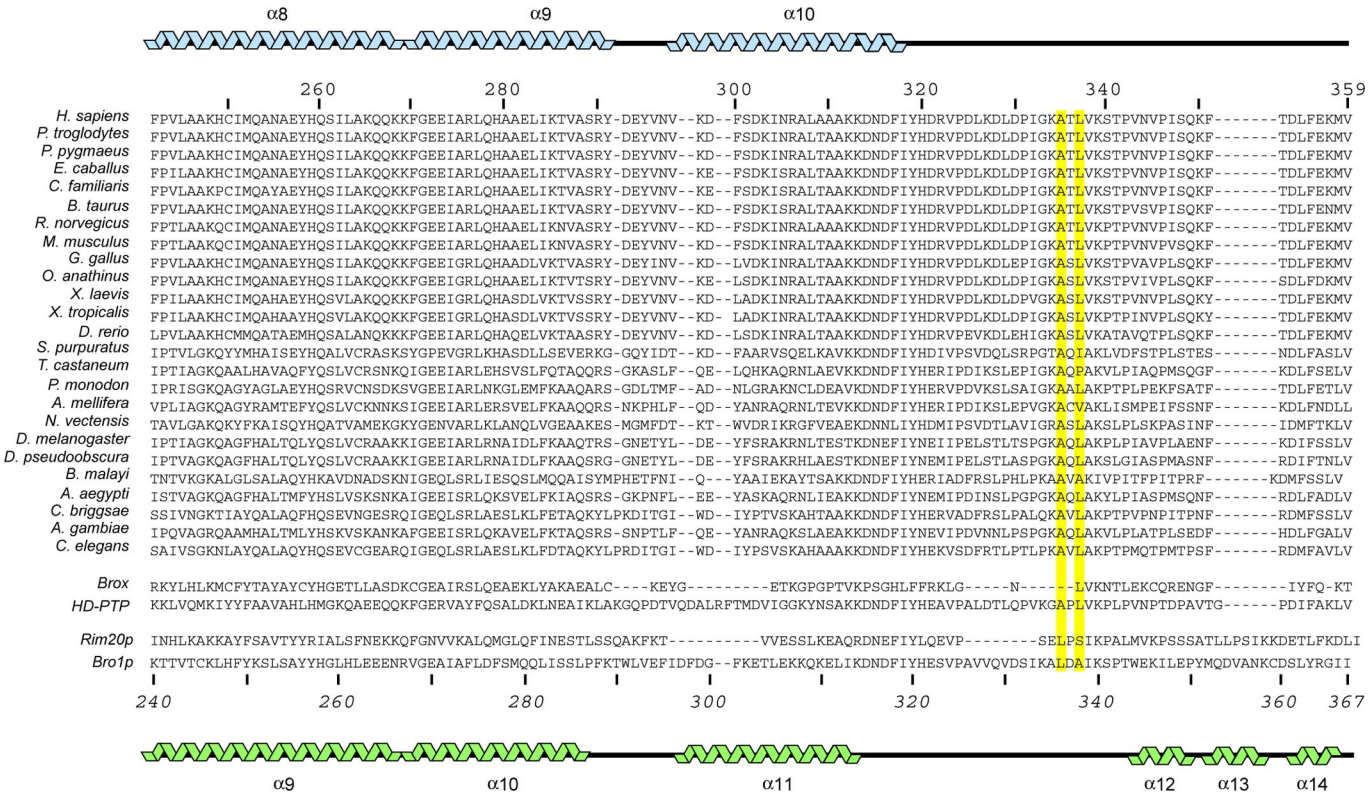

Fig. S4 (Continued). Sequence alignments and secondary structures of Bro1 domains. Secondary structures of the Bro1 domain of ALIX (*Upper*) and Bro1p (*Lower*) (PDB entry 1zb1) are shown together with aligned primary sequences of $ALIX_{Bro1}$ domains from 25 representative metazoan species (top sequence block), Bro1 domains from the human Brox and HD-PTP proteins (middle sequence block), and Bro1 domains from the yeast Rim20p and Bro1p proteins (bottom sequence block). $ALIX_{Bro1}$ and Bro1p were aligned by least squares overlap of the two structures, and other sequence alignments were performed by using the ClustalW server http://npsa-pbil.ibcp.fr/NPSA/npsa_clustalw.html [Combet C, Blanchet C, Geourjon C, Deléage (2000) NPS@: Network protein sequence analysis. *Trends Biochem Sci* 25:147–150]. Residues highlighted in yellow make contacts with CHMP4A in the ALIXBro1-$CHMP4A_{205–222}$ structure and residues italicized in bold and red block ALIX binding and HIV-1 budding when mutated to Asp.

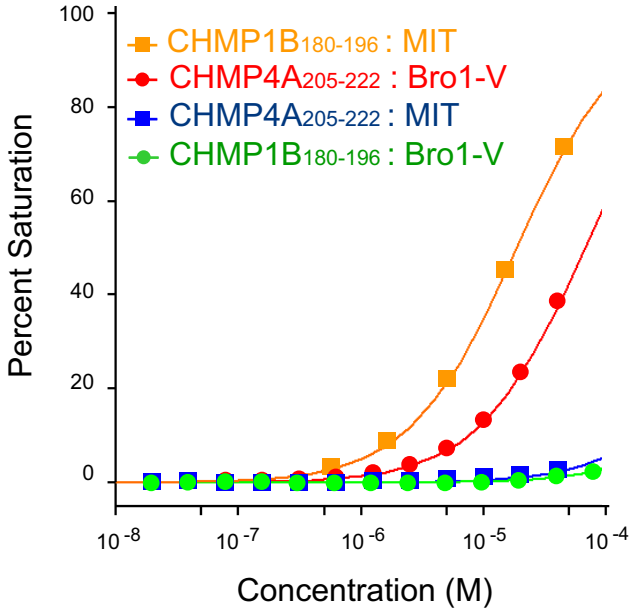

Fig. S5. Selectivity of the CHMP4A and CHMP1B recognition helices for $ALIX_{Bro1-V}$ and Vps4A MIT. Biosensor isotherms showing $ALIX_{Bro1-V}$ and VPS4A MIT domain binding to immobilized GST-$CHMP4A_{205-222}$ and GST-$CHMP1B_{180-196}$. Estimated dissociation constants for $ALIX_{Bro1-V}$ interactions were: GST-$CHMP4A_{205-222}$, 44 $\pm$ 6 μM, GST-$CHMP1B_{180-196}$, $>$ 1 mM. Estimated dissociation constants for VPS4A MIT domain interactions were: GST-$CHMP4A_{205-222}$, $>$ 1 mM, GST-$CHMP1B_{180-196}$, 18.5 $\pm$ 0.6 μM (dissociation constant and error were estimated from a statistical fit of a single binding isotherm derived from duplicate measurements at six different Vps4A MIT domain concentrations over a range of 0–140 μM). Binding to a control GST surface was negligible in all cases (data not shown).

Table S1. Data collection and refinement statistics for $ALIX_{Bro1}$–CHMP4 complexes

Statistic	CHMP4A	CHMP4B	CHMP4C
Data collection			
Space group	C2	C2	C2
Cell dimensions			
a, *b*, *c*, Å	120.7, 62.7, 76.1	120.5, 62.6, 76.1	120.9, 62.4, 76.4
b, deg.	122.1	121.5	121.6
Resolution, Å	50.0–2.15 (2.23–2.15)	50.0–2.1 (2.18–2.10)	50.0–2.02 (2.09–2.02)
R_{sym}	0.063 (0.334)	0.067 (0.413)	0.066 (0.596)
$I/\sigma(I)$	19 (1.8)	14 (1.7)	9 (1.5)
Completeness, %	94.9 (75.1)	92.3 (67.6)	95.5 (81.0)
Redundancy	9.5 (3.8)	7.2 (4.6)	6.6 (4.4)
Refinement			
Resolution, Å	50.0–2.15 (2.21–2.15)	50.0–2.10 (2.154–2.10)	50.0–2.02 (2.07–2.02)
Reflections, no.	25,024	26,458	30,381
R_{work}	0.214 (0.305)	0.228 (0.326)	0.243 (0.333)
R_{free}	0.284 (0.344)	0.290 (0.386)	0.291 (0.411)
Number of atoms			
Protein	2911	2953	2905
Ligand/ion	6	6	6
Water	127	90	56
$\langle B \rangle$-factors			
Protein	33.2	35.3	34.0
Ligand/ion	82.5	78.9	85.8
Water	49.9	55.0	51.3
rmsd			
Bond lengths, Å	0.019	0.017	0.016
Bond angles, deg.	1.710	1.653	1.542
Ramachandran plot, %			
Most favored	89.7	88.0	90.6
Additionally allowed	9.7	10.8	8.6
Generously allowed	0.3 (Q27)	1.2 (K207,Q27,S31,C40)	0.3 (K207)
Disallowed	0.3 (Q88)	0.0	0.6 (Y29, E34)

Diffraction data from one crystal were used to determine each structure. This includes the CHMP4A complex, for which data were collected in two separate sweeps from different beamlines. Values in parentheses refer to the high-resolution shell.

Table S2. Thirty-four different CHMP4 protein sequences from 19 different metazoan species grouped together with the human CHMP4 isoform with which they show the greatest pair-wise identity throughout the entire protein

CHMP4 protein	Organism	NCBI protein accession no.	Overall identity to most homologous human CHMP4, %	C-terminal sequence
4A	*Homo sapiens*	Q9BY43	100	PKVDEDEEA**L**KQ**L**AE**W**VS
4A	*Pan troglodytes*	XP_001169270	99(A)	PKVDEDEEA**L**KQ**L**AE**W**VS
4A	*Canis familiaris*	XP_537387	91(A)	PEADEDEAA**L**KQ**L**AE**W**VS
4A	*Bos taurus*	AAI33472	91(A)	PKADEDEAE**L**KQ**L**AE**W**VS
4A	*Monodelphis domestica*	XP_001380207	81(A)	ASKTDEEKE**M**KQ**L**VD**W**VS
4B	*Homo sapiens*	NP_789782	100	KKKEEEDDD**M**KE**L**EN**W**AGSM
4B	*Mus musculus*	NP_083638	99(B)	KKKEEEDDD**M**KE**L**EN**W**AGSM
4B	*Macaca mulatta*	XP_001105255	99(B)	KKKEEEDDD**M**KE**L**EN**W**AGSM
4B	*familiaris*	XP_542966	97(B)	KKKEEEEDD**M**KE**L**EN**W**AGSM
4B	*Bos taurus*	AAI23448	97(B)	KKKEEEDED**M**KE**L**ET**W**AGTI
4B	*Rattus norvegicus*	XP_001073409	97(B)	KKKEEEDDD**M**KE**L**EN**W**AGSM
4B	*Monodelphis domestica*	XP_001381361	96(B)	KKKEEEDDD**M**KE**L**EN**W**AGSM
4B	*Ornithorhynchus anatinus*	XP_001518785	94(B)	KKKEEEDDD**M**KE**L**EN**W**AGSM
4B	*Equus caballus*	XP_001499057	94(B)	KKKEEEDDD**M**KE**L**EN**W**AGTI
4B	*Gallus gallus*	NP_001006286	91(B)	KKEEEEDDD**M**KE**L**EA**W**AGNM
4B	*Xenopus laevis*	Q5XGW6	87(B)	KKQEEDDDD**M**RE**L**EN**W**ATA
4B	*Xenopus tropicalis*	Q6GL11	87(B)	KKQEEDDDD**M**RE**L**EN**W**ATA
4B	*Danio rerio*	Q7ZVC4	86(B)	KKEEEDEDD**M**KD**L**EA**W**AAN
4B	*Nematostella vectensis*	XP_001639344	67(B)	AKKKTEDDD**L**AE**L**EA**W**AS
4B	*Ornithodoros moubata*	AAS59855	66(B)	SKAVMEDPD**M**IE**L**AQ**W**AS
4B	*Anopheles gambiae*	XP_315330	64(B)	AVAEEDDPD**M**KE**L**MS**W**AN
4B	*Caenorhabditis elegans*	AAA68771	61(B)	PRAKEADKD**L**ED**L**ES**W**AN
4B	*Drosophila melanogaster*	NP_610462	57(B)	AVEDDDDPD**M**KQ**L**LS**W**SN
4C	*Homo sapiens*	Q96CF2	100	QRAEEEDDD**I**KQ**L**AA**W**AT
4C	*Pan troglodytes*	XP_528179	99(C)	RRAEEEDDD**I**KQ**L**AA**W**AT
4C	*Macaca mulatta*	XP_001093735	98(C)	RRAEEEDDD**I**KQ**L**AA**W**AT
4C	*Canis familiaris*	XP_535115	88(C)	SKRTEEVDD**I**KQ**L**AA**W**AP
4C	*Bos taurus*	AAI13332	88(C)	RRTEGEDDD**I**QH**L**AA**W**AT
4C	*Monodelphis domestica*	XP_001367000	88(C)	SRRKEDEDD**I**KQ**L**AA**W**AS
4C	*Equus caballus*	XP_001489156	87(C)	RRAEEDDDD**I**KK**L**SA**W**AT
4C	*Mus musculus*	Q9D7F7	84(C)	SRRAEEDDD**F**KQ**L**AA**W**AT
4C	*Rattus norvegicus*	Q569C1	84(C)	SRRAEEDDD**F**KQ**L**AA**W**AT
4C	*Gallus gallus*	XP_418312	72(C)	RRRVEDEDD**M**KQ**L**AA**W**AS
4C	*Xenopus laevis*	Q6GNN8	69(C)	SKKVEDDDD**M**QM**L**AA**W**AT

Conserved hydrophobic, Leu, and Trp positions in the terminal recognition helix are in bold. For reference, pairwise identities between the three human CHMP4 isoforms are 62% (A vs. B), 52% (A vs. C), and 61% (B vs. C), whereas the nearest identity between a human CHMP4 protein and another human CHMP protein is 30% (CHMP4A vs. CHMP5). Note that our current nomenclature for CHMP4A (NCBI protein accession locus Q9BY43), CHMP4B (NP_789782), and CHMP4C (Q96CF2) matches the current NCBI database annotations (www.ncbi.nlm.nih.gov/sites/entrez) but that the designations of CHMP4A and CHMP4B are reversed from those used in several previous publications.